Boiling effect in crater development on magnesium surface induced by laser melting

Guan, Yingchun; Zhou, Wei; Li, Zhongli; Zheng, Hongyu

2014

Guan, Y., Zhou, W., Li, Z., & Zheng, H. (2014). Boiling effect in crater development on magnesium surface induced by laser melting. Surface and Coatings Technology, 252, 168-172.

https://hdl.handle.net/10356/85036

https://doi.org/10.1016/j.surfcoat.2014.05.002

Boiling Effect in Crater Development on Magnesium Surface Induced by Laser Melting

Yingchun Guan[1,a,b], Wei Zhou[a b], Zhongli Li[b], Hongyu Zheng[b]

[a] Nanyang Technological University, 50 Nanyang Avenue, Singapore 639798

[b] Singapore Institute of Manufacturing Technology, 71 Nanyang Drive, Singapore 638075

[1] Corresponding author: Tel: (65) 6793 8386; Fax: (65) 6791 6377; E-mail: guan0013@e.ntu.edu.sg

Abstract:

This paper demonstrated that micron-craters could be fabricated on both magnesium and Mg alloy surface by nanosecond pulsed laser processing. Experimental results revealed that the craters with broad distribution of dimension occurred after laser melting. Morphological difference at the irradiated surface between Mg and Mg alloy indicated that thermal properties, alloying elements and microstructure of irradiated materials were key factors responsible for crater formation. It was proposed that the craters were formed by combined effect of explosive volume boiling and generation of cavitation bubbles during lase melting. Thermal effect of nanosecond pulsed laser processing on Mg and Mg alloy as well as progressive formation of laser-induced crater was further discussed. Such phenomenon extended potential applications of Mg materials, which offered the potential for developing new types of Mg-based biomedical devices.

Keywords: nanosecond pulse laser, Mg and Mg alloy, crater, boiling and bubble, thermal effect.

1. Introduction

Thermal effect in laser processing is responsible for precision and quality of produced structures on materials. In the past decades, compared to conventional continuous wave laser, pulsed lasers have been developed rapidly due to peak power performances [1-8]. Nanosecond pulsed laser processing with high efficiency and productivity has been considered as promising method in manufacturing industries [2, 3].

When a short-pulse laser beam interacts with metals, thermalization in the electron subsystem is very fast, and electrons are heated to high temperature [1, 2, 5-10]. Correspondingly, surface temperature of irradiated materials increases rapidly. Referring to governing equation in heat transfer and fluid flow model of laser-material interaction [1, 9-11], it is assumed that thermal conductivity for the lattice subsystem is neglected, and electrons can be heated to very high transient temperature. According to the most used models including one-dimensional two-temperature-components model for heat transport inside the metal [2-5] and three-dimensional heat balance equations for temperature distribution as well as threshold energy density calculation [9-11], the main source of energy losses during nanosecond pulse duration is heat diffusion into the irradiated

substrate. Therefore, thermal diffusivity of materials is a key factor responsible for melting and solidification processes. Various structures can be produced at the surface for wide applications.

Magnesium and Mg alloys have been increasingly used in the industries and biomaterial fields due to low density, high specific strength and biodegradability [12-14]. Unfortunately, inferior surface performance is a major factor that limits their actual applications [12, 13, 15]. Previous researchers show significant enhancement of surface properties including wear and corrosion resistance on laser-irradiated Mg alloys, mainly because laser can produce surface layers with fine microstructure that reduce size of galvanic couples and expand solid solution range of alloying elements [11, 15-18].

In this paper, we firstly report the capability of nanosecond pulsed laser to achieve local boiling phenomenon and micro-sized crater formation at Mg surface without chemical composition change. The laser used has a top-hat beam profiler with scanning mode, which is suitable for large area melting due to high power density and uniform energy distribution. We demonstrate how thermal effect occur over a large area of irradiated surface and discuss the influence of materials with laser processing on morphology as well as dimension of the crater. We conclude by explaining the mechanism of crater formation during laser-Mg interaction, and indicate how it applies for potential applications.

2. Experimental Procedures

The materials studied were as-cast Mg and AZ91D Mg alloy with the following chemical composition (wt.%): Al 8.97, Zn 0.78, Mn 0.31, Si 0.023, Cu 0.002, Ni 0.0005 and Mg balance. The specimens of dimension of 30 mm by 30 mm by 3 mm were extracted from the ingot, ground with progressively finer SiC paper (180, 400, 800, 1200, 2400 and 4000 grit) to minimize the effect of incidence angle, and cleaned with alcohol.

A nanosecond pulsed Nd:YAG laser (ROFIN DQ ×50 S, wavelength 1064 nm, pulse duration 43 ns, repetition rate 12 000 Hz) was used in this study. The average power density was 2.15×10^{8} W/cm^2 (heat flux 1.85 J/cm^2 per pulse). The laser beam was delivered normal to the specimen surface through an optical fiber and galvanometer scanner. The square beam spot size was focused as 0.6 mm side length at the sample surface. The laser scanning speed was varied as 100 mm/s, 500 mm/s and 1000 mm/s to study the effect of laser energy on surface evolution of irradiated materials, and the corresponding laser pulse number for single spot is 72, 7.2, 3.6, respectively. The irradiated area was 10×10 mm^2 in square using hatched scanning mode with 50% overlapping in the program. When laser was turned on, the specimen was placed in a well-sealed chamber using 2.0 bar Ar (2.0×10^{5} Pa) gas flow to minimize oxidation, as shown in Figure 1.

After laser irradiation, surface topography of irradiated area was measured using Talysurf stylus profilometer, and microstructural features were examined by Scanning Electron Microscope (JEOL 5600 LV) equipped with Energy Dispersive Spectroscopy. The EDS measurements provided information on the chemical composition.

3. Results

Figure 2 displays effect of nanosecond pulsed Nd:YAG laser melting on Mg and Mg alloy surface. Various craters and their development occur at both surfaces. Diameter evolution of the craters with the decreasing laser scanning speed is in the range of 10-50 μm for Mg alloy and 10-25 μm for Mg, respectively. It also shows that typical shape of the crater is a combination of conical profile with ripples at the wall of conical crater. Tiny pores can be found at the wall of the crater on Mg alloy surface at a slow scanning speed. Moreover, molten materials surrounding the craters were observed at the surface, and it increased with the decreasing laser scanning speed significantly. It has been suggested that micron-sized droplets are resulted from hydrodynamic instability of the molten liquid layer during laser melting [10], and the molten mass is pushed radially outward from the irradiated area. This is in good agreement with our results, as shown in high magnification figures of the craters in Figure 2.

Surface topography of the craters was further investigated. The diameter of Mg craters is 10-25 μm and diameter of Mg alloy craters is 10-50 μm, which is the same as SEM results in Figure 2. Depth range of the craters was found to be 10-150 μm for Mg alloy and 5-100 μm for Mg, respectively. The results of surface topography measurement reveal that Mg alloy surface melt further than that of Mg irradiated by incident laser light.

Cross-sectional views of laser-irradiated surface were also examined. Figure 3(a) presents that melt depth is around 20 μm for Mg alloy at fast scanning speed as 1000 mm/s, which is much shallower than 150 μm induced by millisecond pulse Nd:YAG laser according to previous study [11, 18, 19]. Few cellular/dendrite microstructures were found in both the melt layers. Figure 3(b) shows that the molten materials can be seen clearly inside the crater, and Figure 3(c) reveals big pores at the wall of the crater. Figure 3(d) observes a large amount of melt drop on Mg at slow scanning speed as 100 mm/s, and no obvious phase change as well as pores was found in the microstructure. Melt depth for Mg and Mg alloy in Figure 3(c) and (d) is around 100 μm.

Quantitative analyses of elementary compositions based on EDS found that Al content in all melted layers of Mg alloy was in the range of 10.2-11.1 wt%, which was slightly higher than the average value of 9.0 wt% in the untreated substrate. This was due to relatively more Mg element vaporization during laser irradiation [11, 18, 19]. According to experimental work, the combined effect of various craters and less solidification microstructure as well as Al concentration in the melt layer resulted in no improvement of surface properties of AZ91D alloy following nanosecond pulse Nd:YAG laser irradiation. In addition, no change of chemical composition was observed for Mg samples.

4. Discussions

4.1 Thermal Effect

At nanosecond pulse duration, excited electrons created by incident laser radiation transfer energy to phonons during electron-phonon relaxation, and the energy will be redistributed through lattice vibrations of metal. Consequently, heat is conducted into the irradiated substrate [1, 2, 5]. As mentioned in the introduction, thermal diffusivity of the material is crucial for producing structures. Thermal diffusivity of Mg and AZ91D alloy is calculated as 8.468×10^{-5} m^2/s and 2.894×10^{-5} m^2/s, respectively [12, 13], while melting point of Mg and AZ91D alloy is 650˚C and 595˚C [12, 13], respectively. Thereby, more molten materials occurs at the irradiated surface of AZ91D alloy compared to that of Mg under the same laser fluence, as shown in Figure 2.

Temperature distribution curve for single laser pulse can be calculated from transient heat balance equation based on the heat flow model [9-11]. Results show that surface temperature of irradiated Mg and AZ91D alloy increases rapidly from room temperature to peak temperature near to 4000 ˚C within pulse duration 43 ns. Such rapid heating will lead to explosive boiling because liquid Mg can be heated above its normal boiling temperature (boiling point of Mg and AZ91D alloy is 1091˚C and 1107˚C [12, 13], respectively) and become highly superheated. According to foundation on explosive boiling established by Martynyuk and Kelly [20, 21], superheated liquid metal experiences large density fluctuations, and these fluctuations can generate vapour bubbles in the entire superheated liquid layer. Once bubbles of size exceed critical radius, they undergo rapid transition into a mixture of vapor and liquid droplets. Such process is termed as explosive boiling.

Threshold energy density for explosive boiling on Mg and AZ91D alloy can also be estimated from the heat flow model [11, 22, 23]. Critical temperature of Mg was assumed as 5000 K as average value for common metals due to lack of available data. Based on the value for optical and thermal properties of Mg and AZ91D alloy in the literature [12, 13, 24], the calculated threshold value on both surfaces would be 2.41×10^{8} W/cm^2 and 1.48×10^{8} W/cm^2, respectively. Due to the presence of well-sealed chamber with 2.0 bar Ar gas flow, plasma shielding effect decreases significantly compared to laser radiation in atmosphere environment [22, 25]. Therefore, current average power density 2.15×10^{8} W/cm^2 is sufficient to induce explosive boiling.

4.2 Crater Formation

The development of crater formation is illustrated in Figure 4. During nanosecond pulsed laser irradiation, incident light at high fluence created a large population of heat at the surface of materials. The conducted heat was accumulated to melt the materials and generate superheated metastable liquid layer, as shown in Figure 4(a) and (b). Driven by pressure and temperature difference above irradiated surface, it is generally accepted that plasma expansion is accompanied by emission of shock waves in chamber environment [2, 26]. Plasma expanded adiabatically at a supersonic velocity, creating high-pressure shock waves in front of it, as shown in Figure 4(c).

Highly superheated layer lead to mixture of vapor and liquid droplets occur, resulting in explosive boiling accompany with vapour bubbles expansion [20-23]. Nucleation of gaseous phase such as defects, particles, alloying element sites took place at the near surface, leading to “microexplosions” of the material during incoming laser pulse. According to Craciun *et al.* [27, 28],

these “microexplosions” inside the target would cause volume expulsion of the material (see Fig. 1 in Ref. 27 and Fig. 4 in Ref. 28). Moreover, liquid layer at Mg and AZ91D alloy surface was measured as 20-100 μm on basis of Figure 2 and Figure 3, indicating sufficient time to allow vapor bubbles to grow spontaneously to critical size [22].

As the laser plasma cooled, the shock front rapidly detached from the plasma because its velocity was much greater than the particle velocity behind it [22, 29]. Subsequently, the laser induced bubbles caused by explosive boiling continued to expand outward until all its initial kinetic energy was converted into potential energy. Under the external pressure of the liquid materials, the bubbles began to implode adiabatically. The bubble’s rebound would occur since both temperature and pressure inside the liquid layer raise again during laser overlapping scan processing. Usually a bubble oscillated for several cycles until all the energy was dissipated and all gases dissolve into the surrounding liquid, especially for multiply laser pulses. The oscillation of bubble resulted in the conical profile with ripple structures at the wall (Figure 2 and Figure 3). As a consequent, a typical micron-sized crater was formed, as show in Figure 4(d).

The melted matter caused by the volume expulsion could act as “fresh” defects, lead to a next preferential laser irradiation for craters formation [30, 31]. In such a way, many gathered cluster of craters were formed within the molten materials after several consecutive laser pulses, which resulted in various sizes of the craters at the surface (Figure 2(a)). On the other hand, displaced molten material returned to its original place due to gravitational forces and surface tension during rapid cooling process at the end of heating cycle [1, 2, 22]. Finally, rough molten material accompany with micron-sized craters generated a distinct topography at the surface of Mg and AZ91D alloy, as show in Figure 4(e).

In addition, it is known that formation of crown-like structures is produced by radial liquid flow, which is attributed to laser-induced plasma-recoil pressure pushing melt toward outer periphery of melt pool under the regime of hydrodynamic flow [2, 22, 23]. The recoil pressure is principally temperature dependent phenomenon. With the increasing energy density, temperature increased significantly, leading to higher recoil pressure that in turn created higher velocity and bigger bubbles in the molten material. As a consequence, thick melt layer with expanded bubbles was formed on the surface at slow scanning speed, as shown in Figure 2 and Figure 3. When heavy liquid flow companied with the bubble oscillation at AZ91D alloy surface, it was difficult for gases to be dissolved completely into the liquid. Thereby, pores left inside the molten materials and craters, as shown in Figure 2(b).

Therefore, we propose that the various craters and the molten materials are caused by laser-induced explosive volume boiling. More craters take place for AZ91D alloy possibly due to the combined results of lower thermal diffusivity, lower melting point including secondary β-$Mg_{17}Al_{12}$ phase 450 ˚C, alloying element and particle sites (Figure 3). It should be noted that such craters were also obtained on the irradiated surface of wrought AZ31B alloy following the same laser processing, but total number of craters was in the between of AZ91D alloy and Mg. Further effort is needed to elucidate the detailed relationship between alloying elements of materials and subsurface superheating as well as explosive volume boiling, and to identity the mechanism of crater formation.

5. Conclusions

Occurrence of micron-sized craters was observed on Mg and Mg alloy surface following by nanosecond pulsed Nd:YAG laser melting. Typical morphology of the crater was a combination of conical profile with ripples present at the wall of the crater, which was possibly attributed to the oscillation of bubble at high temperature and pressure above the surface during laser irradiation. More molten materials occurred on Mg alloy compared to that of Mg, and alloying element Al content in all melted layers of Mg alloy was higher than that in the untreated substrate due to selective vaporization. It was suggested that various craters were mainly formed as a result of laser-induced explosive volume boiling and cavitation bubbles generation. Thermal properties, alloying elements and microstructures of the materials determined final amount and dimension of the craters at the irradiated surface. By adjusting laser parameters according to thermal properties of materials, this technique can be applied in many applications, which offers the potential for developing new types of Mg-based biomedical devices.

Acknowledgments

Support by Nanyang Technological University, Ph.D. scholarship and Singapore Institute of Manufacturing Technology, A*STAR (Agency for Science, Technology and Research, Singapore), Collaborative Research Project U11-M-030AU is gratefully acknowledged.

References

[1] P. Peercy, Solidification dynamics and microstructure of metals in pulsed laser irradiation, in: C.W. Draper, P. Mazzoldi (Eds.), Laser Surface Treatment of Metals, Kluwer Academic Publishers, Boston, 1986, pp 57-78.

[2] H.G. Rubahn, Laser Applications in Surface Science and Technology, John Wiley & Sons, 1999.

[3] W.M. Steen, Laser industry: an Introduction to laser processing and its industrial application, in: Jack Lawrence, J. Pou, D. K. Y. Low, E. Toyserkani, Advances in laser materials processing, Woodhead Publishing, CRC Press, 2010, pp 3-17.

[4] X. Zhang, S.S. Chu, J.R. Ho, C.P. Grigoropoulos, Excimer laser ablation of thin gold films on a quartz crystal microbalance at various argon background pressures, Appl. Phys. A 64(1997) 545-52.

[5] N.M. Bulgakova, A.V. Bulgakov, Pulsed laser ablation of solids: Transition from normal vaporization to phase explosion, Appl. Phys. A 73(2001) 199-208.

[6] B. Lan, M.H. Hong, S.X. Chen, K.D. Ye, Z. Wang, G.X. Chen, T.C. Chong. Laser-ablation-induced concentric ring structures, Jpn. J. Appl. Phys. (Part 1) 42(2003) 5123-6.

[7] W.D. Song, M.H. Hong, B. Lukyanchuk, T.C. Chong, Laser-induced cavitation bubbles for cleaning of solid surfaces, J. Appl. Phys. 95 (2004) 2952.

[8] Z.L. Li, T. Liu, C.C. Khin, A.C. Tan, L.E. Khoong, H.Y. Zheng, W. Zhou, Direct patterning in sub-surface of stainless steel using laser pulses, Opt. Express 18(2010) 15990.

[9] X. He, P.W. Fuerschbach, T. DebRoy, Heat transfer and fluid flow during laser spot welding of 304 stainless steel, J. Phys. D: Appl. Phys. 36(2003) 1388-98.

[10] P.S. Wei, C.N. Ting, J.S. Yeh, T. DebRoy, F.K. Chung, G.H. Yan, Origin of wavy weld boundary, J. Appl. Phys. 105 (2009) 053508.

[11] Y.C. Guan, W. Zhou, Z.L. Li, H.Y. Zheng, Study on the solidification microstructure in AZ91D Mg alloy after laser surface melting, Appl. Surf. Sci. 255(2009) 8235-8.

[12] S. Housh, B. Mikucki, A. Stevenson, Properties of Magnesium Alloys, Properties and Selection: Nonferrous Alloys and Special-Purpose Materials, ASM Handbook ASM International, 1990.

[13] S.C. Erickson, Magnesium in Properties and Selection: Nonferrous Alloys and Special-Purpose Materials, Materials Park, Ohio, 2002.

[14] F. Witte, The history of biodegradable magnesium implants: A review, Acta Biomaterialia 6(2010) 1680-92.

[15] J.E. Gray, B. Luan, Protective coatings on magnesium and its alloys-a critical review, J. Alloys. Comp. 336 (2002) 88-113.

[16] G. Abbas, Z. Liu, P. Skeldon, Corrosion behaviour of laser-melted magnesium alloys, Appl. Surf. Sci. 247(2005) 347-53.

[17] H.C. Man, S. Zhang, F.T. Cheng, X. Guo, In situ formation of a TiN/Ti metal matrix composite gradient coating on NiTi by laser cladding and nitriding, Surf. Coat. Technol. 200 (2006) 4961-6.

[18] Y.C. Guan, W. Zhou, H.Y. Zheng, Effect of laser surface melting on corrosion behaviour of AZ91D in Simulated-modified Body Fluid, J. Appl. Electrochem. 39(2009) 1457-64.

[19] Y.C. Guan, W. Zhou, H.Y. Zheng, Z.L. Li, Solidification microstructure of AZ91D Mg alloy after laser surface melting, Appl. Phys. A 101(2010) 339-44.

[20] A. Peterlongo, A. Miotello, R. Kelly, Laser-pulse sputtering of aluminum: vaporization, boiling, superheating, and gas-dynamic effects, Phys. Rev. E 50 (1994) 4716-27.

[21] A. Miotello, R. Kelly, Critical assessment of thermal models for laser sputtering at high fluences, Appl. Phys. Lett. 67 (1995) 3535.

[22] J.H. Yoo, S.H. Jeong, R. Greif, R.E. Russo, Explosive change in crater properties during high power nanosecond laser ablation of silicon, J. Appl. Phys. 88 (2000) 1638.

[23] N. Ozisik , Heat Conduction, Wiley, New York, 1993.

[24] J.R. Davis, (Ed.) Engineered Materials Handbook Desk Edition, Engineering Data for Metals and Alloys, ASM Handbook, ASM International, 2002.

[25] X. Mao, R. Russo, Observation of plasma shielding by measuring transmitted and reflected laser pulse temporal profiles, Appl. Phys. A. 64(1997) 1-6.

[26] D. Bhattacharya, F.L.K. Singh, P.H. Holloway, Laser-target interactions during pulsed laser deposition of superconducting thin-films, J. Appl. Phys. 70(1991) 5433-9.

[27] V. Craciun, D. Craciun, Evidence for volume boiling during laser ablation of single crystalline target, Appl. Surf. Sci. 138(1999) 218-23.

[28] V. Craciun, N. Bassim, R.K. Singh, D. Craciun, J. Hermann, C. Boulmer-Leborgne, Laser-induced explosive boiling during nanosecond laser ablation of silicon, Appl. Surf. Sci. 186(2002) 288-92.

[29] J.W.M. Jacobs, J.M.G. Rikken, Boiling effects and bubble formation at the solid-liquid interface during laser-induced metal-deposition, J. Electrochem. Soc. 134 (1987) 2690-6.

[30] H. Li, S. Costil, V. Barnier, R. Oltra, O. Heintz, C. Coddet, Surface modifications induced by nanosecond pulsed Nd:YAG laser irradiation of metallic substrates, Surf. Coat. Technol. 201(2006) 1383-92.

[31] M. Holmes-Cerfon, W. Zhou, A.L. Bertozzi, M.P. Brenner, M.J. Aziz, Development of Knife-Edge Ridges on Ion Sputtered Surfaces, Appl. Phys. Lett. 101 (2012) 143109.

Figure captions

Fig. 1 Schematic diagram of experimental setup

Fig. 2 SEM images of laser-induced craters on Mg and AZ91D alloy surfaces by nanosecond pulsed Nd:YAG laser irradiation at different scanning speeds: (a) 1000 mm/s on Mg; (b) 100 mm/s on Mg; (c) 1000 mm/s on AZ91D alloy; and (d) 100 mm/s on AZ91D alloy.

Fig. 3 SEM images showing the cross-sectional views of craters at AZ91D alloy and Mg surfaces by nanosecond pulsed Nd:YAG laser melting: (a) craters in the melted layer of AZ91D alloy at 1000 mm/s scanning speed; (b) high magnification of (a); (c) craters in the melted layer of AZ91D alloy at 100 mm/s scanning speed; (d) craters in the melted layer of Mg at 100 mm/s scanning speed.

Fig. 4 Schematic representation showing the stages of laser-induced crater formation: (a) surface absorption and thermal conduction; (b) surface melting (boiling); (c) plasma expansion and shock waves; (d) cavitation bubble generation; (e) bubble oscillation and crater formation.

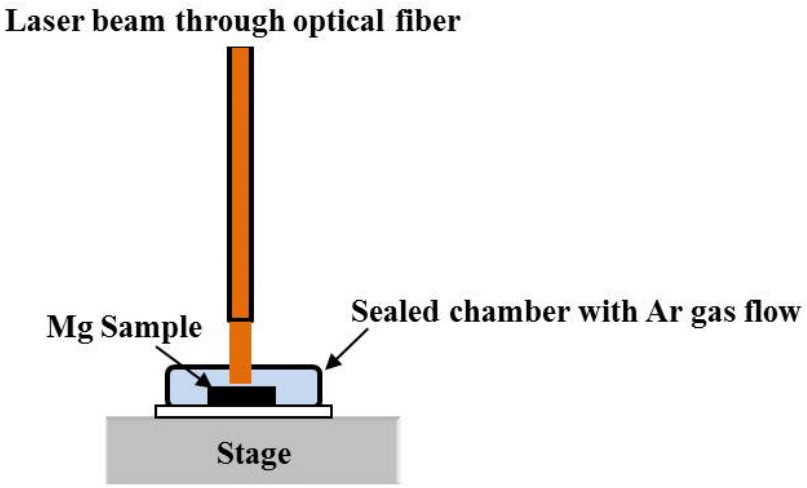

Fig. 1

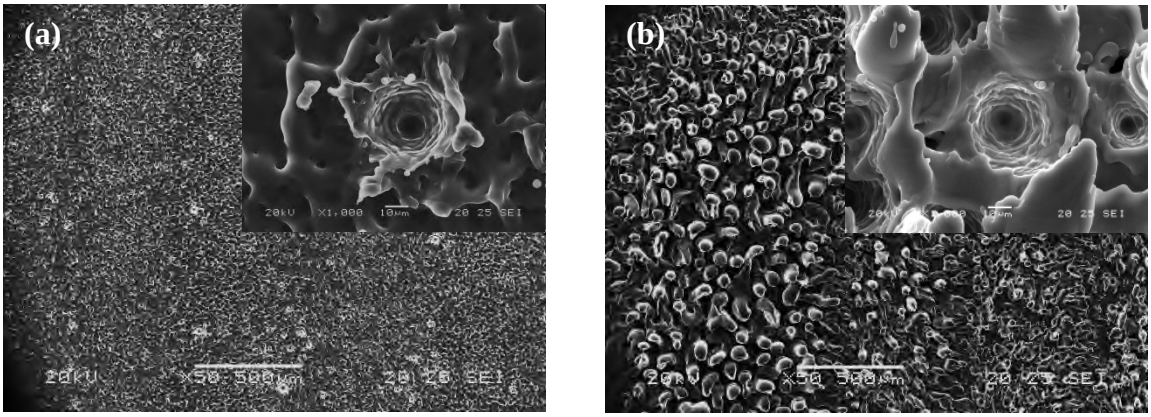

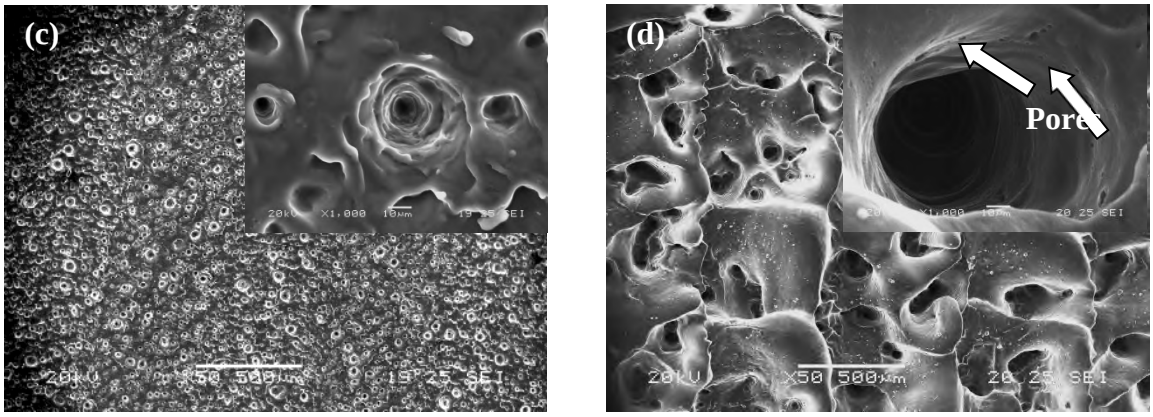

Fig. 2

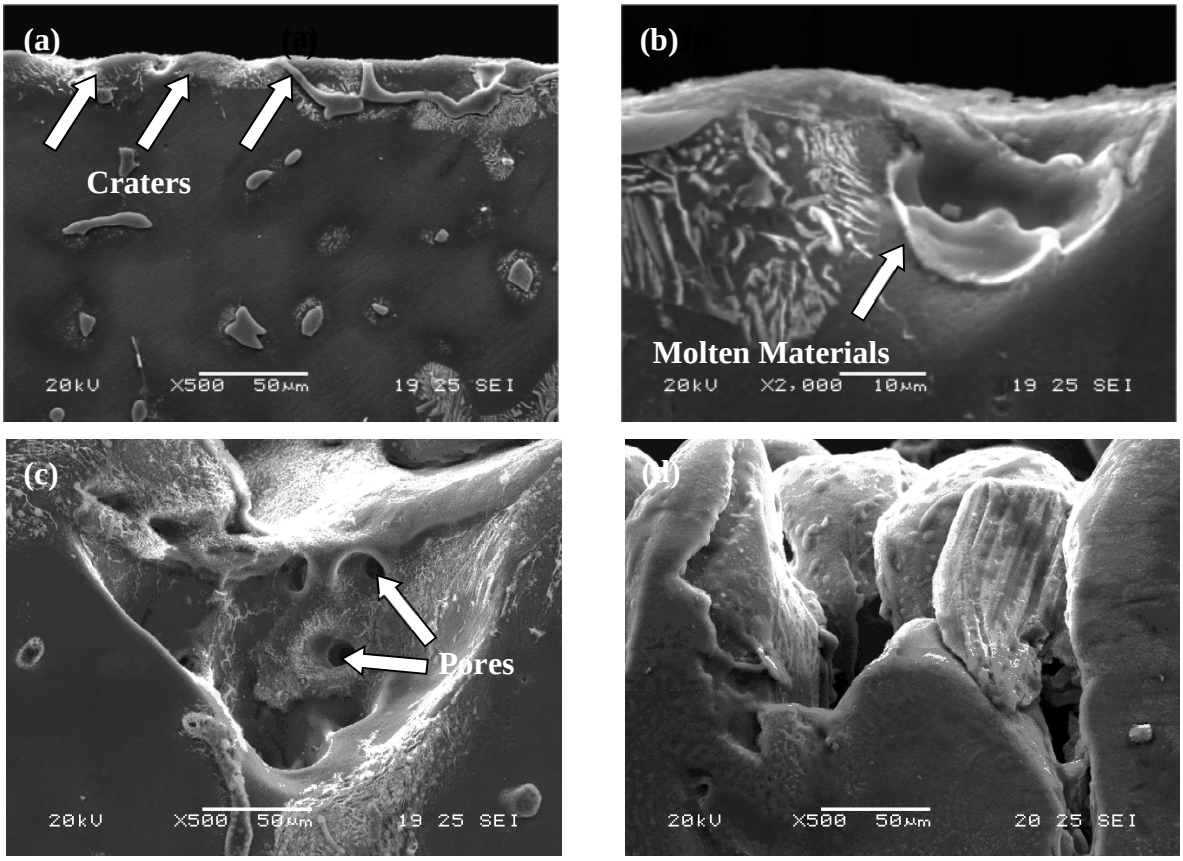

Fig. 3

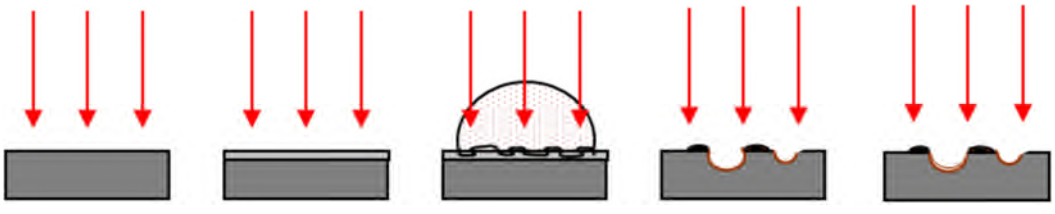

Fig. 4